Lamb, GP and Kobayashi, S

GRB 170817A as a jet counterpart to gravitational wave trigger GW 170817

Lamb, GP and Kobayashi, S (2018) GRB 170817A as a jet counterpart to gravitational wave trigger GW 170817. Monthly Notices of the Royal Astronomical Society, 487 (1). pp. 733-740. ISSN 0035-8711

Monthly Notices of the ROYAL ASTRONOMICAL SOCIETY
MNRAS **478,** 733–740 (2018) doi:10.1093/mnras/sty1108
Advance Access publication 2018 May 1

GRB 170817A as a jet counterpart to gravitational wave trigger GW 170817

Gavin P. Lamb[1,2★] and Shiho Kobayashi[1]
[1]*Astrophysics Research Institute, LJMU, IC2, Liverpool Science Park, 146 Brownlow Hill, Liverpool L3 5RF, UK*
[2]*Department of Physics and Astronomy, University of Leicester, University Road, Leicester LE1 7RH, UK*

Accepted 2018 April 11. Received 2018 April 11; in original form 2017 October 12

ABSTRACT
Fermi/GBM (Gamma-ray Burst Monitor) and *INTEGRAL* (the International Gamma-ray Astrophysics Laboratory) reported the detection of the γ-ray counterpart, GRB 170817A, to the LIGO (Light Interferometer Gravitational-wave Observatory)/*Virgo* gravitational wave detected binary neutron star merger, GW 170817. GRB 170817A is likely to have an internal jet or another origin such as cocoon emission, shock-breakout, or a flare from a viscous disc. In this paper we assume that the γ-ray emission is caused by energy dissipation within a relativistic jet and we model the afterglow synchrotron emission from a reverse and forward shock in the outflow. We show the afterglow for a low-luminosity γ-ray burst (GRB) jet with a high Lorentz factor (Γ); a low-Γ and low-kinetic-energy jet; a low-Γ, high-kinetic-energy jet; structured jets viewed at an inclination within the jet-half-opening angle; and an off-axis 'typical' GRB jet. All jet models will produce observable afterglows on various time-scales. The late-time afterglow from 10 to 110 d can be fitted by a Gaussian structured jet viewed at a moderate inclination, however the GRB is not directly reproduced by this model. These jet afterglow models can be used for future gravitational wave detected neutron star merger counterparts with a jet afterglow origin.

Key words: gravitational waves – gamma-ray burst: general – gamma-ray burst: individual: GRB 170817A.

1 INTRODUCTION

Short γ-ray bursts (GRBs) are thought to be due to internal energy dissipation (e.g. Meszaros & Rees 1993; Kobayashi, Piran & Sari 1997; Daigne & Mochkovitch 1998; Zhang & Yan 2011) in an ultrarelativistic jet launched when rapid accretion of material by a compact merger object occurs following a binary neutron star (NS–NS) or neutron star black hole (NS–BH) merger (e.g. Eichler et al. 1989; Paczynski 1990; Kluźniak & Lee 1998). The NS–NS/BH merger is due to the loss of orbital energy and angular momentum via gravitational radiation (e.g. Phinney 1991). This makes such systems a candidate for gravitational wave (GW) detection by advanced LIGO (Light Interferometer Gravitational-wave Observatory)/*Virgo* (Abbott et al. 2016). The detection of a GRB in association with a GW signal is key to confirming the neutron star binary merger scenario as the progenitor for short GRBs.

GRB 170817A, with an isotropic equivalent γ-ray energy $E_\gamma = (4.0 \pm 0.98) \times 10^{46}$ erg at $\sim$40 Mpc, a duration for 90 per cent of the γ-ray energy $T_{90} \sim 2 \pm 0.5$ s, and a νF_ν spectral peak energy $E_p = 185 \pm 62$ keV (Connaughton et al. 2017; Goldstein et al. 2017a,b; Savchenko et al. 2017a,b) was detected by *Fermi*/GBM (Gamma-ray Burst Monitor) and *INTEGRAL* (the International Gamma-ray Astrophysics Laboratory) as a potential electromagnetic (EM) counterpart to the binary NS merger GW 170817 (Abbott et al. 2017a,b) with a delay of $\sim$2 s from the GW detection to the GRB. From the GW signal, the system is inclined with an angle $0^\circ \le i \le 36^\circ$ from the line of sight (Abbott et al. 2017c), where the inclination i gives the angle between the rotational axis and the observer. Using known constraints on H_0 the inclination is $3^\circ \le i \le 23^\circ$ with the Planck $H_0 = 67.74 \pm 0.46$ km s^{-1} Mpc^{-1} (Planck Collaboration XIII 2016), and $14^\circ \le i \le 32^\circ$ using the Type Ia supernova measurements from SHoES $H_0 = 73.24 \pm 1.74$ km s^{-1} Mpc^{-1} (Riess et al. 2016); more recently, an inclination of $i = 18^\circ \pm 8^\circ$ using H_0 from the Dark Energy Survey was found by Mandel (2017).

The Swope Supernova Survey detected an optical counterpart (SSS17a) in association with the galaxy NGC4993, 10.9 h post-merger (Coulter et al. 2017). The counterpart was consistent with a blue kilo/macro-nova from the dynamical merger ejecta (e.g. Tanaka et al. 2014; Metzger et al. 2015; Barnes et al. 2016; Tanaka 2016; Wollaeger et al. 2017). See also (Arcavi et al. 2017; Covino et al. 2017; Cowperthwaite et al. 2017; Drout et al. 2017; Evans et al. 2017; Gall et al. 2017; Kilpatrick et al. 2017; Nicholl et al. 2017;

★ E-mail: gpl6@le.ac.uk

Pian et al. 2017; Shappee et al. 2017; Smartt et al. 2017; Tanaka et al. 2017; Tanvir et al. 2017; Valenti et al. 2017, etc.). If GRB 170817A was from internal dissipation within a compact merger jet, then the GRB would be accompanied by an afterglow. In this paper we calculate the expected flux at various frequencies from a forward and reverse shock. We model the afterglow from a low-luminosity GRB jet, a low Lorentz factor (Γ) jet, structured jets with either a two-component, power law, or Gaussian structure, and a GRB seen off-axis from a homogeneous jet with typical parameters.

In Section 2 the jet models and parameters used to predict the afterglows are described. In Section 3 we discuss the results and their implications for GRB 170817A, and in Section 4 we give final comments.

2 AFTERGLOW PREDICTION

Energy dissipation within an ultrarelativistic jet that results in a GRB will be followed by a broad-band afterglow as the jet decelerates in the ambient medium; depending on the jet parameters, the peak magnitude and time-scale at various frequencies can vary significantly. By assuming that GRB 170817A was from a compact-merger jet viewed either within or outside the jet opening angle we can make reasonable predictions for the expected afterglow. A forward-shock afterglow is expected to accompany all on-axis GRBs, although a reverse shock may also be present at early times and typically at low frequencies.

In the following section we calculate the afterglow from forward and reverse shocks for a high Lorentz factor, low-kinetic-energy GRB jet (e.g. Sari, Piran & Narayan 1998; Sari, Piran & Halpern 1999; Kobayashi & Sari 2000), and for low Lorentz factor, low and high-kinetic-energy jets (e.g. Lamb & Kobayashi 2016). We also calculate a forward-shock afterglow for various jet structure models viewed off the central axis, and a homogeneous jet viewed outside the jet-half-opening angle (e.g. Lamb & Kobayashi 2017).

2.1 High-Γ, low-kinetic-energy jet

Using the isotropic γ-ray energy reported by *Fermi* for GRB 170817A, $E_\gamma = (4.0 \pm 0.98) \times 10^{46}$ erg, and making reasonable assumptions for the afterglow parameters, a prediction can be made for the expected flux at various frequencies. The typical parameters for a sample of short GRBs are given by Fong et al. (2015), who find that the ambient density is $n\sim$ (3–15)$\times$ 10^{-3} cm^{-3}, and the γ-ray efficiency[1] is $0.4 \lesssim \eta \lesssim 0.7$. As the γ-ray luminosity of GRB 170817A is well below the typical values for a short GRB, we extend the efficiency range to a lower limit of 0.1; for a jet with an efficiency lower than 0.1, see the discussion at the end of Section 2.2. From the efficiency and γ-ray energy the jet kinetic energy can be determined, $E_{\rm k} = E_\gamma(1/\eta - 1)$; the jet kinetic energy drives the afterglow. The accelerated particle distribution index for short GRBs is $p = 2.43^{+0.36}_{-0.28}$ (Fong et al. 2015), we use $p = 2.5$ as our fiducial value. Other assumed jet parameters are the jet bulk Lorentz factor, $\Gamma = 80$, and the microphysical parameters, $\epsilon_B = 0.01$ and $\epsilon_e = 0.1$. Note that these parameters are assumed throughout unless otherwise stated.

The duration of the GRB can be used to indicate the width of the relativistic shell, $\Delta_0 \sim cT_{90}$ (Kobayashi et al. 1997), where we assume that the GRB is from internal dissipation processes and c is the speed of light. If the bulk Lorentz factor is below a critical value $\Gamma_c = (3E_{\rm k}/32\pi n m_p c^2\Delta_0^3)^{1/8}$, then the reverse shock cannot effectively decelerate the shell; here m_p is the mass of a proton. For short GRBs the reverse shock is typically described by the thin shell case. The shell crossing time for such a reverse shock is $\sim(\Gamma/\Gamma_c)^{-8/3}T_{90}$ and the characteristic frequency for the reverse shock is $\nu_{m,RS} \sim \nu_{m,FS}/\Gamma^2$ (Kobayashi 2000), where subscripts RS and FS indicate reverse and forward shocks, respectively, and $\nu_{m,FS}$ is the forward-shock characteristic frequency. The spectral peak flux at the characteristic frequency is proportional to the number of electrons, the magnetic field, and the bulk Lorentz factor. The mass in the shell is a factor Γ larger than the heated and swept up ambient density of the forward-shock region. The spectral peak flux for the reverse shock is then $F_{\nu,{\rm max},RS} \sim \Gamma F_{\nu,{\rm max},FS}$. The forward- and reverse-shock regions can have a different pre-shock magnetization parameter ϵ_B, for simplicity we assume that they are the same.

At low frequencies synchrotron self-absorption becomes important; for the reverse shock, synchrotron self-absorption will limit the flux more efficiently than for the forward shock because the effective temperature of the electrons in the reverse-shock region is lower by a factor $\sim\Gamma$. The limiting flux, at a given frequency ν and observer time t, for the reverse shock is (e.g. Kobayashi & Sari 2000)

$$F_{\nu,{\rm BB}} \sim 2\pi m_p c^2 \Gamma^3 D^{-2} \varepsilon_e t^2 \nu^2 \left(\frac{p-2}{p-1}\right)\left(\frac{e}{\rho}\right) \times \max\left[\left(\frac{\nu}{\nu_{m,RS}}\right)^{1/2}, 1\right], \quad (1)$$

where e is the internal energy density and ρ is the mass energy density in the reverse-shock region. At the shock crossing time $(e/\rho) \sim 1$ and $(e/\rho) \propto t^{-2/7}$ after the shock crossing. For the forward shock, the limiting flux is a factor Γ larger at the shock crossing time.

If the ejecta from the central engine is magnetized, ϵ_B in the reverse-shock region would be higher than that in the forward-shock region. The higher ϵ_B will make the reverse shock peak slightly later and brighter. At early times and low frequencies, synchrotron self-absorption limits the reverse-shock emission. As the reverse-shock region expands, the emitting surface becomes larger, and the flux limit grows as $F_{\nu,{\rm BB}} \propto t^{1/2}$ (see Kobayashi & Sari 2000; Kopač et al. 2015, for the blackbody approximation), where $\nu < \nu_{m,RS}$. When this limit becomes higher than the synchrotron flux $F_\nu \propto \varepsilon_B^{1/3} t^{-1/2}$ (Kobayashi 2000), the reverse-shock component peaks. Note that the self-absorption limit does not depend on ϵ_B, but the synchrotron flux does. By equalizing the two flux estimates, we find that the peak time and peak flux of the reverse-shock emission are scaled as $\varepsilon_B^{1/3}$ and $\varepsilon_B^{1/6}$, respectively. If $\nu > \nu_{m,RS}$, these scalings are $F_{\nu,{\rm BB}} \propto t^{9/7}$ and $F_\nu \propto \epsilon^{(p+1)/4} t^{-2}$. We find the peak time and flux are scaled as $\varepsilon_B^{(p+1)/4}$ and $\varepsilon_B^{(p+1)/10}$, respectively. For low-Γ outflows, synchrotron self-absorption is less important and the reverse shock will peak at the time when the shock crosses the shell. If $\nu_{m,RS} < \nu$ at peak time, then the peak time and flux are proportional to $\varepsilon_B^{(p-1)/4}$ and $\varepsilon_B^{3(p-1)/4}$ (e.g. Zhang & Kobayashi 2005; Kobayashi et al. 2007).

[1]The efficiency of the prompt emission from an internal shock origin is usually given by $\eta \sim f_{\rm dis}\epsilon_e f_{\rm rad}$, where the fraction of energy dissipated is $f_{\rm dis} \lesssim 0.5$ and the fraction of energy radiated is $f_{\rm rad} \sim 1$. Using $\epsilon_e = 0.1$, the value of the efficiency should be $\eta \lesssim 0.05$. However, the value estimated from an internal shock efficiency can be much higher if we consider the collision of multiple shells with a broad range of Lorentz factors (Kobayashi & Sari 2001). The resultant light curve would appear smoother and broader for a large number of shells. We base our estimates first on the central observed values of η found for short GRBs by Fong et al. (2015), where the range of observed efficiencies is $10^{-3} \lesssim \eta \lesssim 0.98$.

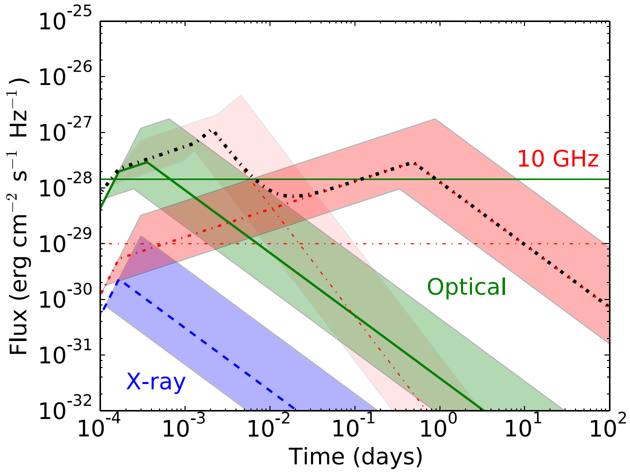

Figure 1. Afterglow light curves for a jet with an isotropic γ-ray energy of 4.0×10^{46} erg, a γ-ray efficiency of $\eta = 0.4$, a jet bulk Lorentz factor $\Gamma = 80$, in an ambient medium of $n = 0.009\,\mathrm{cm}^{-3}$ with microphysical parameters $\epsilon_B = 0.01$ and $\epsilon_e = 0.1$, and a luminosity distance of 40 Mpc. The blue dashed line shows the X-ray afterglow, the green solid line shows the optical afterglow, and the red dash–dotted line shows the 10 GHz radio afterglow. The shaded regions indicate the light curve for an efficiency $0.1 \le \eta \le 0.7$. The reverse shock is important at radio frequencies, the 10 GHz reverse shock is shown as a thin dash–dotted red line and faint shaded region for the range of jet energies considered; the forward and reverse shocks light curve at 10 GHz is shown as a thick black dash–dotted line. The red dashed horizontal line indicates the 1μJylimit, the green horizontal dashed line indicates $m_{AB} \sim 21$ mag, and lower limit of the y-axis is the X-ray sensitivity $\sim$0.4 μCrab at 4 keV.

The forward-shock light curve will evolve as $t^{-3(p-1)/4}$ after the peak.

A jet viewed on-axis will exhibit a light curve break when $\Gamma^{-1} < \theta_j$ (Sari et al. 1999), where θ_j is the jet-half-opening angle. As $\Gamma \propto E^{1/8}\, n^{-1/8}\, t^{-3/8}$, the break time should occur at

$$t_j \sim 10\, E_{\mathrm{k},50}^{1/3} n_{-2}^{-1/3} (\theta_j/0.31)^{8/3}\ \mathrm{d}, \tag{2}$$

where subscripts follow the convention $N_x = N/10^x$, θ_j is in radians and we normalize to a jet with $\theta_j = 0.31$ rad, or $\sim 18°$. Note that for GRB 170817A to be on-axis, i.e. within the jet opening angle, the value of θ_j should be larger than the system inclination. For jets where the kinetic energy is $\lesssim 10^{48}$ erg, or the half-opening angle is $\lesssim 6°$, then the jet will break at $\sim$1 d. Where the energy is low and the jet is narrow, then the break will occur at $\sim$0.1 d. The jet-half-opening angle is unknown, however as the inclination is $\sim 18°$ (Mandel 2017) this can be used to indicate a wide jet if the GRB is observed on-axis. The jet-break is not included in the analysis.

The afterglow light curve for a jet viewed on-axis is shown in Fig. 1; the ambient density is set as the mean of the Fong et al. (2015) sample, $n = 0.009\,\mathrm{cm}^{-3}$. Before the deceleration time, when Γ is constant, the forward-shock flux and characteristic frequency depend on the ambient density as $[F_{\nu,\max}, \nu_m] \propto n^{1/2}$. The deceleration time depends on the number density as $t_{\mathrm{dec}} \propto n^{-1/3}$. After the deceleration time, $\nu_m \propto t^{-3/2}$ and the dependence on the ambient density vanishes. Where $\nu < \nu_m$ at the deceleration time, the light curve will continue to increase as $F_\nu = F_{\nu,\max}(\nu/\nu_m)^{1/3}$ until $\nu = \nu_m$, the peak here is therefore $F_\nu \propto n^{1/2}$ as ν_m no longer depends on n.

Afterglow light curves are shown for 10 GHz, optical, and X-ray frequencies. The shaded regions represent the uncertainty in the γ-ray efficiency $0.1 \le \eta \le 0.7$. The bold afterglow lines show the light curve for a γ-ray efficiency $\eta = 0.4$, where the dash–dotted red line is 10 GHz, the solid green line is optical (5×10^{14} Hz), and the dashed blue line is X-ray (10^{18}Hz). The reverse-shock emission is shown as a thin dash–dotted red line with a faint shaded region; and the reverse and forward shocks afterglow at 10 GHz assuming the mean efficiency is shown as a thick black dash–dotted line. The forward shock dominates emission for optical and X-ray frequencies. As a reference, the horizontal dash–dotted line shows 1 µJy, horizontal solid line shows $m_{\mathrm{AB}} = 21$, and the approximate *Swift*/XRT (X-Ray Telescope) limit is given by the lower limit of the y-axis at 10^{-32} erg cm^{-2} s^{-1} Hz^{-1}.

2.2 Low-Γ jets

The minimum radius at which the prompt γ-ray photons can be emitted is the photospheric radius, where the outflow becomes optically thin. The photospheric radius is given by

$$R_p = \left[\frac{\sigma_T E_{\mathrm{k}}}{4\pi m_p c^2 \Gamma}\right]^{1/2} \sim 1.9 \times 10^{13} E_{\mathrm{k},50}^{1/2} \Gamma_1^{-1/2}\ \mathrm{cm}, \tag{3}$$

where σ_T is the Thomson cross-section.

Considering the relatively high E_p despite the low L_γ we assume that the prompt γ-ray photons are emitted near the photosphere. The observed delay time between the GW signal and the GRB is equivalent to the traveltime for a constant Lorentz factor flow to a radial distance equivalent to the photospheric radius, $\Delta t \sim R_p/2\Gamma^2 c$. The bulk Lorentz factor is then

$$\Gamma = \left[\frac{(\sigma_T E_{\mathrm{k}})^{1/2}}{4\Delta t c^2 \left(\pi m_p\right)^{1/2}}\right]^{2/5} \sim 12\, E_{\mathrm{k},50}^{1/5} \left(\frac{\Delta t}{2\ \mathrm{s}}\right)^{-2/5}, \tag{4}$$

where Δt is the measured delay time.

The prompt γ-ray emission is predicted to be suppressed for a jet with a low Lorentz factor, the higher energy emission will be suppressed due to pair production and the total energy in the photons reduced due to adiabatic cooling before decoupling from the expanding plasma at the photosphere[2] (e.g. Hascoët et al. 2014; Lamb & Kobayashi 2016). GRB 170817A had a thermal component (Goldstein et al. 2017b) that would be expected from photospheric emission (e.g. Pe'er, Mészáros & Rees 2006a). To reflect the possible prompt suppression we extend the lower limit of the γ-ray efficiency range.[3] The Lorentz factor for a jet with $0.001 \le \eta \le 0.7$, and the observed E_γ, from equation (4), is $10.0 \gtrsim \Gamma \gtrsim 2.2$. The afterglow light curves from low-Γ jets are shown in Fig. 2; we use an efficiency of $\eta = 0.1$ for the light curve. The shaded region indicates the afterglow for the limits of the efficiency.

The low-Γ value for the outflow gives a relatively long deceleration time (t_{dec}) for the jet, where $t_{\mathrm{dec}} \propto \Gamma^{-8/3}$. The reverse shock will cross the shell at $\sim$0.4–1.7 d for $10 \gtrsim \Gamma \gtrsim 2.2$, respectively. At radio frequencies the reverse-shock emission will dominate over the forward-shock light curve at t_{dec} for $\Gamma \gtrsim 5$. This will result in a brightening of the light curve before the forward shock peak due to the reverse shock. The reverse shock is only important at early times and for the upper limits of the parameter space; the reverse shock is shown for the 10 GHz light curves in Fig. 2.

[2]This suppression results in the fraction of energy radiated being $f_{\mathrm{rad}} < 1$, while the assumed value for ϵ_e remains unchanged.

[3]Where the efficiency is high, the jet kinetic energy will be low and suppression of dissipated energy within a low-Γ outflow reduced (see Lamb & Kobayashi 2016). Such low-energy, low-luminosity, and low-Γ jets may form a distinct population (e.g. Siellez et al. 2016).

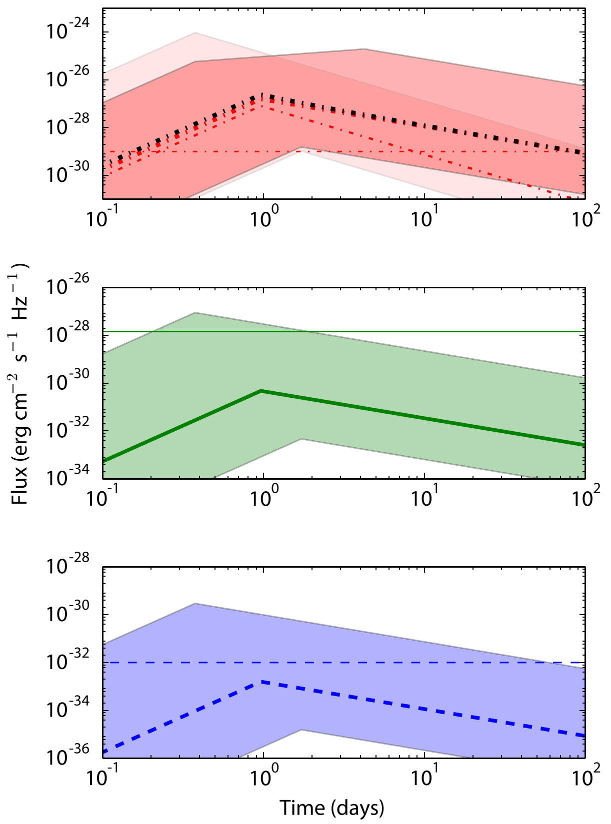

Figure 2. Afterglow from a low-Γ jet with an isotropic γ-ray energy of 4.0×10^{46} erg, a γ-ray efficiency of $0.001 \le \eta \le 0.7$ and a luminosity distance 40 Mpc. The jet bulk Lorentz factor is estimated from the delay time as $2.2 \lesssim \Gamma \lesssim 10.0$, all other parameters are as Fig. 1. The lines show the afterglow for a jet with $\Gamma \sim 3.9$, the shaded regions indicate the uncertainty in the kinetic energy and the Lorentz factor. Colours are as for Fig. 1. *Top* panel: 10 GHz emission where the thin dash–dotted line and faint shaded region indicate the reverse shock; the thick dash–dotted line and shaded region indicate the forward shock; the sum of reverse- and forward-shock light curves is shown as a black dash–dotted line. The red horizontal dashed line indicates the 1 μJy limit. *Middle* panel: optical afterglow. The green solid line shows the optical magnitude 21. *Bottom* panel: X-ray afterglow. The blue horizontal dashed line is ~0.4 μCrab at ~4 keV.

The level of suppression of the prompt emission is unknown; if all jets from binary neutron star mergers produce jets with a similar kinetic energy (e.g. Shapiro 2017), then the afterglow would appear brighter than a low-luminosity jet afterglow with a typical η value. Using a jet kinetic energy of $E_{\rm k} = 10^{52}$ erg, the bulk Lorentz factor from equation (4), would be $\Gamma \sim 30$ and the prompt emission significantly suppressed (e.g. Lamb & Kobayashi 2016). The prompt efficiency for such a jet would be very low, $\eta \sim 10^{-6}$, where the observed GRB had energy equivalent to GRB 170817A. The afterglow for such a jet is shown in Fig. 3; as the jet kinetic energy is fixed, here the limits of the shaded regions represent the uncertainty on the ambient medium number density, $n\sim (3-15)\times 10^{-3}$ cm^{-3}. A reverse shock is apparent at 10 GHz, peaking at ~2 d with a flux ~10 Jy; the reverse shock is shown in the figure as a thin red dash–dotted line with the associated uncertainty in the ambient number density. A black dash–dotted line indicates the sum of the 10 GHz light curve from the forward and reverse shocks.

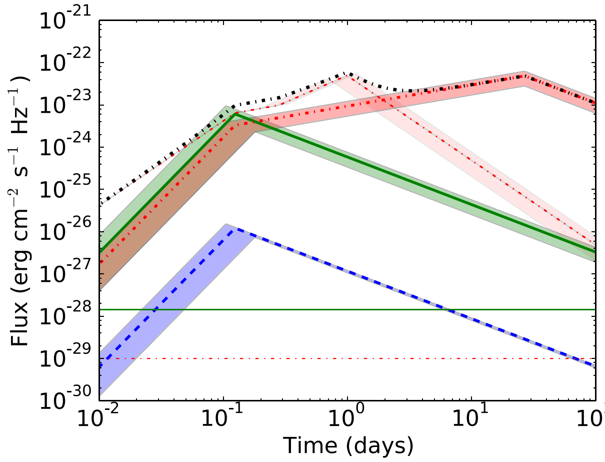

Figure 3. Afterglow from a low-Γ jet with a jet kinetic energy of 10^{52} erg, and a luminosity distance 40 Mpc. The jet bulk Lorentz factor is estimated from the delay time as $\Gamma \sim 30$. Shaded regions represent the range of ambient densities $(3 \lesssim n \lesssim 15) \times 10^{-3}$ cm^{-3}, all other parameters are as Fig. 1. The reverse shock at 10 GHz is shown as a thin dash–dotted red line and faint shaded region. Colours are as for Fig. 1. The green horizontal solid line is optical m_{AB}= 21, and the red horizontal dash–dotted line indicates the 1 μJy limit.

2.3 Structured jet

GRBs are usually assumed to have a homogeneous, or 'top-hat', structure, i.e. the energy and Lorentz factor are uniform in a jet cross-section and the jet has a sharp edge defined by the jet-half-opening angle. However, jets may have some intrinsic structure either due to the formation and acceleration processes or as a result of jet breakout from merger ejecta. Here we use the structured jet models from Lamb & Kobayashi (2017); see also Xiao et al. (2017) for a similar analysis or Jin et al. (2017) and Kathirgamaraju, Barniol Duran & Giannios (2018) for discussion of the prompt emission from a structured jet. For each of the three models used the total isotropic equivalent jet core energy is fixed at 10^{52} erg, and the core extends to an angle of 6° from the central axis. The jet parameters, E and Γ, vary according to the model: for a two-component jet, E and Γ are at 5 per cent of the core values between 6° and 25°; for a power-law jet, E and Γ vary with angle outside the core following a power-law index -2; and for a Gaussian structured jet the parameters E and Γ depend on angle following a Gaussian function from 0° to 25°. The detected prompt emission in a 50–300 keV band is determined for each jet model at observation angles from 0° to 25° and a distance 40 Mpc. The observation angle values are selected for each jet structure where the detected prompt photon flux is comparable to the observed *Fermi*/GBM and *INTEGRAL*. The prompt emission from each jet component is calculated considering the angle to the line of sight, and the dissipation and photospheric radius in each case. The flux at the detector is determined by considering the photon arrival times and the emission duration. The afterglow from each model for the determined inclination is then generated following the method in Lamb & Kobayashi (2017).

The Gaussian jet model, shown in Fig. 4 (left-hand panel), has an inclination of 18°.5. For the power-law jet model, shown in Fig. 4 (central panel), the inclination angle is 25°.5. For the two-component model, shown in Fig. 4 (right-hand panel), the inclination angle is 11°; note that for the two-component model the γ-ray emission is that seen off-axis from the core jet region, the wider sheath component has a low-Γ value such that the prompt emission is fully

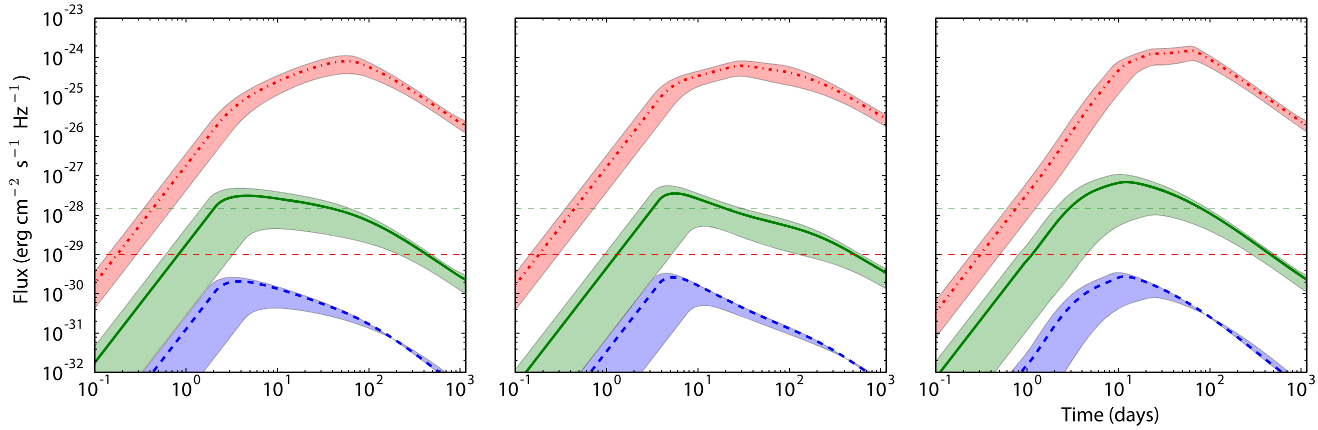

Figure 4. Afterglows from jets with structure; jet core parameters are $E_{\rm iso} = 10^{52}$ erg, $\eta = 0.4$, $\Gamma = 80$, and $\theta_c = 6°$, all other parameters are as previously used. The jet structure extends to 25° in each case. *Left*: Gaussian structure, a Gaussian function on E and Γ with angle from the centre. Jet inclined to the observer at 18°.5. *Middle*: Power-law structure with a decay index outside of the core of $k = -2$. Jet inclined to the observer at 25°.5. *Right*: Two-component structure, where the second component has 5 per cent of the core parameters. Jet inclined to the observer at 11°.

suppressed. In the figure the afterglow at 10 GHz is shown in red with a dash–dotted line, optical is shown in green with a solid line and X-ray is shown in blue and with a dashed line. The shaded region represents the uncertainty in the ambient medium number density, with the line indicating the afterglow for the mean $n = 0.009\,{\rm cm}^{-3}$.

For each model the first break in the light curve is due to the deceleration time for the jet component inclined towards the observer, i.e. the jet component at the inclination angle. At radio frequencies, the light curve will peak when the characteristic frequency crosses the observation band, $\nu_m = \nu$. At optical and X-ray frequencies, and at radio frequencies for the two-component jet, a late-time excess or a shallow decay is due to the off-axis emission from the bright core of the jet. Any late-time break in the light curve is due to the edge of the jet becoming visible, i.e. the jet-break, equation (2).

For the structured jet models the photon flux at the detector from the prompt emission approximates, without fine-tuning, the observed parameters: for the Gaussian jet the prompt fluence is $\sim 3.8 \times 10^{-7}$ erg cm^{-2}; for the power-law jet the prompt fluence is $\sim 7 \times 10^{-7}$ erg cm^{-2}; and for the two-component jet the prompt fluence is $\sim 2.1 \times 10^{-7}$ erg cm^{-2}. The *Fermi*/GBM measured fluence is $(2.8 \pm 0.2) \times 10^{-7}$ erg cm^{-2} (Abbott et al. 2017b; Goldstein et al. 2017b). The difference in fluence between the jet models and the observed value is due to the choice of numerical resolution. The fluence for each jet model was calculated in 0°.5 steps from 0° to 28° and the inclination for the jet determined by the angle for which the fluence was closest to the observed value. The observed spectral shape, or peak value, was not calculated in this estimation.

2.4 Off-axis afterglow

The T_{90} duration of GRB 170817A is longer than the typical value of $\sim$0.6 s (Zhang et al. 2012), although still within the usual period for short GRB classification $\lesssim$2 s. The delay time between the GW signal and the detected prompt emission, and the duration and low luminosity of the γ-rays could be due to the jet inclination to the line of sight, where for an off-axis observer the time until emission and the duration are lengthened from that for an on-axis observer by the relativistic Doppler factor, $t \propto \delta^{-1}$ where t is the observed time, $\delta = [\Gamma(1 - \beta\cos\theta_{\rm obs})]^{-1}$ is the Doppler factor and β the velocity as a fraction of c, and the observed fluence is $\propto \delta^3$ (e.g. Ioka & Nakamura 2001). The off-axis prompt emission will also appear to be brighter in X-rays (e.g. Yamazaki, Ioka & Nakamura 2002).

If the jet is inclined in such a way that the observer's line of sight is outside of the jet edge, i.e. $\theta_{\rm obs} > \theta_j$, then the prompt and afterglow emission will be delayed and suppressed when compared to that seen by an on-axis observer, i.e. $\theta_{\rm obs} \rightarrow 0$. In considering an observer at various angles from the jet central axis, we use the method in Lamb & Kobayashi (2017) which includes the jet geometry and emission surface to determine the inclination at which the prompt γ-ray photons have a similar fluence.[4] At an inclination of 11° for a jet with $\theta_j = 6°$, $E_{\rm iso} = 10^{52}$ erg, an efficiency $\eta = 0.4$, and a $\Gamma = 80$, the simplest estimate of the fluence in a T_{90} period from our model is 2.1×10^{-7} erg cm^{-2}. The corresponding afterglow in an ambient medium 0.003 cm^{-3} $\le n \le 0.015\,{\rm cm}^{-3}$ is shown in Fig. 5, where the colours are as previous figures. Note that as $\nu_a < \nu < \nu_m$ at the deceleration time for the 10 GHz light curve, then the synchrotron self-absorption frequency 0.25 GHz $\lesssim \nu_a \lesssim$ 0.75 GHz at this time will not affect the light curve (Sari et al. 1999).

Given an observed $E_p \sim$ 185 keV and the inclination, jet-half-opening angle and Γ used, the 'on-axis' spectral peak energy would be a few MeV. Short GRBs with a spectral peak of a few MeV include GRB 061006, 070714, and 090510; where the $E_p = [955 \pm 267,\ 2150 \pm 1113,\ \text{and}\ 8370 \pm 760]$keV, respectively (e.g. Zhang et al. 2012; Piron 2016). All of these GRBs have high luminosities for short GRBs, where $L_\gamma > 10^{52}$ erg s^{-1}. The high on-axis E_p value applies to the two-component jet discussed in Section 2.3, where the wider sheath component has no detectable γ-ray emission and only contributes to the afterglow light curve.

3 DISCUSSION

By assuming that the observed GRB is from a compact merger jet, we have shown the expected afterglow light curves for various jet models. If GRB 170817A was a low-luminosity GRB viewed

[4]We do not change any of the prompt energy parameters from the model in Lamb & Kobayashi (2017) except the total isotropic energy, efficiency, and bulk-Lorentz factor, where we use $E = 10^{52}$erg, $\eta = 0.4$, and $\Gamma = 80$ instead of $E = 2 \times 10^{52}$erg, $\eta = 0.1$, and $\Gamma = 100$. This maintains consistency with earlier scenarios and avoids fine-tuning.

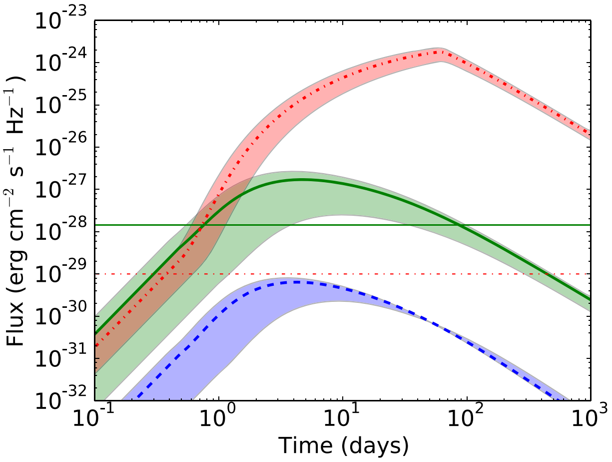

Figure 5. Off-axis afterglow from a homogeneous jet with $E_{\rm iso} = 10^{52}$ erg, $\eta = 0.4$, $\Gamma = 80$, and a half-opening angle $\theta_j = 6^\circ$. The observed γ-ray fluence in the 50–300 keV band is 2.1×10^{-7} erg cm^{-2}; the inclination from the jet central axis is 11° and the ambient density is in the range 0.003 cm$^{-3} \le n \le 0.015$ cm^{-3}.

on-axis, the afterglow in X-ray and optical would peak within seconds of the GRB. A reverse shock in the radio, typically fainter than $\lesssim$1 mJy at 10 GHz, may be visible peaking on a time-scale of minutes; this will be followed by the radio forward-shock afterglow peak with flux $\lesssim$0.1 mJy at $\sim$1 d, i.e. Fig. 1. The predicted optical afterglow is fainter than $m_{AB} \lesssim 19$, and the X-ray afterglow is detectable by *Swift*/XRT but will fade rapidly. The X-ray afterglow will peak within seconds and typically last $\sim$15 min before becoming too faint for *Swift*/XRT, where we assume an X-ray limit of $>10^{-32}$ erg cm^{-2} s^{-1} Hz^{-1}. Such a fast and faint transient would be challenging to detect.

By considering the delay time from GW signal to GRB, constraints can be put on the jet bulk Lorentz factor, if the jet is inclined within the half-opening angle, i.e. on-axis. The energy dissipated will decouple from the jet when the optical depth becomes unity, at the photospheric radius. By using an assumed γ-ray efficiency, the jet kinetic energy can be estimated and from this and the delay time a value for Γ found. The bulk Lorentz factor found using an efficiency $0.001 \le \eta \le 0.7$ is $10.0 \ge \Gamma \ge 2.2$, respectively. This is consistent with the low-Γ jet model of Lamb & Kobayashi (2016), where the prompt emission is expected to be significantly suppressed. The forward-shock afterglow from such a jet is shown in Fig. 2; the afterglow peak in all bands is $\lesssim$1 d and optical and X-ray are faint. Radio emission at 10 GHz is typically $\lesssim$1 mJy and would be detectable for $\gtrsim$1$-$100 d.

If the γ-ray efficiency is very low, i.e. the jet kinetic energy is $E_{\rm k} \gg E_\gamma$, then the derived bulk Lorentz factor, using $E_{\rm k} = 10^{52}$ erg, is $\Gamma \sim 30$. This value is consistent with the low-Γ jet model, predicting suppression of the prompt emission resulting in a low-luminosity GRB. The afterglow for such a jet is shown in Fig. 3; the peak afterglow is typically a few hours after the GRB at optical and X-ray frequencies. Radio, optical, and X-ray emissions are bright in all cases. The 10 GHz afterglow remains at the $\sim$1 Jy level for $\sim$10$-$1000 d, while optical and X-ray fade rapidly.

A jet with extended structure may naturally produce low-luminosity GRBs at wider angles where the jet energetics are lower. By following the structured jet models of Lamb & Kobayashi (2017), we show the expected afterglow from a jet with these models where the observed γ-ray flux is equivalent to the detected *Fermi* value. The afterglows from a Gaussian jet viewed at $i = 18\overset{\circ}{.}5$, a power-law jet viewed at $i = 25\overset{\circ}{.}5$, and a two-component jet viewed at an inclination $i = 11^\circ$ are shown in Fig. 4. Radio, optical, and X-ray emissions are bright in all cases with optical and X-ray light curves peaking $\sim$3$-$100 d and 10 GHz at $\sim$20$-$100 d at the 0.1–1 Jy level. Various features are distinct for each jet model: the Gaussian jet has an early peak with a shallow rise or decline in optical and X-ray emission for $\sim$100 d before breaking to a more rapid decline. In addition the radio typically peaks at the break. For an observer at a wider inclination, the afterglow light curve will show a slow rise from a few days to a peak at $\gtrsim$100 d at all frequencies (e.g. Lamb & Kobayashi 2017). The power-law jet has a sharp early peak at optical and X-ray frequencies whilst the 10 GHz afterglow has a later peak with a slower increase in flux after the deceleration time. Finally the two-component jet has a softer peak and shows a slight rebrightening at late times, especially at radio frequencies, before a rapid decline.

An observer at an inclination just higher than the jet's half-opening angle will see the relativistically beamed prompt and afterglow emission at a later time and at a lower frequency and intensity. The observed delay in the prompt emission and the low-luminosity can be explained by the jet inclination; the afterglow in such a case would be similarly delayed and fainter. We show the afterglow for an observer at 11° from the jet central axis, where the jet has a half-opening angle $\theta_j = 6^\circ$, an isotropic equivalent blast energy 10^{52} erg, a γ-ray efficiency of $\eta = 0.4$, and $\Gamma = 80$. The X-ray afterglow, at $\sim$4 keV, rises slowly to a peak flux $\lesssim 10^{-30}$ erg cm^{-2} s^{-1} Hz^{-1} at $\sim$30 d; optical afterglow has a similar rise index and peak time with a $m_{AB} \lesssim 16$; while the 10 GHz afterglow has a steeper rise rate, breaking to a soft peak from 70 d, the 10 GHz afterglow is brighter than 1 μJy from $\gtrsim$1 to 2 d and peaks at $\sim$1 Jy.

A neutron star binary merger is expected to produce a kilo/macro-nova that will peak with a thermal spectrum at optical to near-infrared frequencies during the first 10 d (e.g. Tanaka et al. 2014; Metzger et al. 2015; Barnes et al. 2016; Tanaka 2016; Wollaeger et al. 2017). For the structured or off-axis jet afterglows, the optical emission may peak on a similar time-scale to the expected kilo/macro-nova. However X-ray and radio emission will reveal the afterglow in such a case. Non-detections by X-ray and/or radio searches for an afterglow from GRB 170817A at early, $<$10 d, times can be used to rule out the various structured and high-kinetic-energy with low-Γ jet scenarios presented here.

The prompt emission for GRB 170817A was fitted by an exponential cut-off power law, the Comptonization spectrum model (e.g. Yu et al. 2016), with a νF_ν spectral peak energy at $E_p \sim 185 \pm 62$ keV, and an index $\alpha \sim -0.62 \pm 0.40$ (Abbott et al. 2017b; Connaughton et al. 2017; Goldstein et al. 2017a,b; Savchenko et al. 2017b). Due to the sparsity of high-energy photons, the requirement for an ultrarelativistic bulk Lorentz factor is relaxed. Additionally, with this E_p and low luminosity, the GRB does not fit on the E_p –L_γ correlation for all GRBs (e.g. Yonetoku et al. 2010; Zhang et al. 2012). A structured jet where the photospheric emission is treated more precisely could explain the GRB (Meng et al. 2018), or the γ-rays could be due to inefficient particle acceleration, wider angle Comptonized emission, or scattered jet internal prompt emission (Kisaka, Ioka & Nakamura 2015; Kisaka et al. 2017). Alternatively the detected γ-ray flux may not have been from a jet but a more isotropic outflow (e.g. Salafia, Ghisellini & Ghirlanda 2018); a cocoon or shock-breakout (Pe'er, Mészáros & Rees 2006b; Lazzati et al. 2017a; Nakar & Piran 2017; Gottlieb, Nakar & Piran 2018), or a flare due to fragmentation of a viscous disc (Perna, Armitage & Zhang 2006).

4 CONCLUSIONS

We have modelled the afterglow from various jet dynamical scenarios given the observed γ-ray flux detected by *Fermi* and *INTEGRAL* for GRB 170817A in association with the GW signal GW 170817. Four scenarios were considered: (i) an on-axis low-luminosity GRB with typical high Lorentz factor; (ii) low-Γ jets viewed on-axis; (iii) jets with extended structure where the prompt emission would have an energy similar to that observed; and (iv) an off-axis jet where the prompt emission is geometrically corrected to give the observed γ-ray fluence. In all cases an afterglow is expected on various timescales and with a range of peak fluxes. Where the kinetic energy is typical for a GRB jet, the afterglow for either a low-Γ jet or from a structured jet where the prompt γ-ray emission is suppressed or low, will result in a bright afterglow, easily detectable at all frequencies. If GRB 170817A is from within a relativistic jet then the jet must be either

(i) a low-energy jet with either a low- or high-Γ, and a high-γ-ray efficiency $\eta \gtrsim 0.4$
(ii) a GRB jet viewed off-axis

If the jet is the first of these, then a large population of low-luminosity, low-energy jets from neutron star mergers could exist resulting in a high-GW detection rate for neutron star mergers.

4.1 An evolving afterglow

X-ray and radio counterparts have been initially reported from ~ 9 to 18 d post-merger (Corsi et al. 2017; Hallinan et al. 2017; Margutti et al. 2017; Mooley, Hallinan & Corsi 2017; Troja et al. 2017). Radio counterparts are expected from the merger ejecta at late times (e.g. Hotokezaka et al. 2016). However, the X-ray and radio observations from ~ 10 to 100 d (Haggard et al. 2017; Hallinan et al. 2017; Margutti et al. 2017; Mooley et al. 2017; Ruan et al. 2017) and recent optical data (Lyman et al. 2018) are consistent with a Gaussian structured jet. One phenomenological fit is for an observer at $\sim 20°$, and with the parameters used in Section 2.3 tuned (e.g. Lyman et al. 2018; Margutti et al. 2018), the jet energy structure is a modified Gaussian profile, $e^{-\theta^2/\theta_c^2}$ and a Gaussian profile for the Lorentz factor, $e^{-\theta^2/2\theta_c^2}$. The parameters for the afterglow shown in Fig. 6 are $E_{\rm k} = 10^{52}$erg and $\Gamma = 80$ for the jet core with an angle $\theta_c = 4\overset{\circ}{.}5$, microphysical parameters $\epsilon_e = 0.01$ and $\epsilon_B = 0.01$, $p = 2.1$, and $n = 10^{-3}\,{\rm cm}^{-3}$, where the range indicates an observer between $10° \leq i \leq 26°$ (Mandel 2017) and the thick lines indicate 20°. The GRB emission is not directly reproduced by this model, however the contribution from scattered prompt emission of the jet core (Kisaka et al. 2017) or other higher latitude effects have not been considered. Alternatively a jet-cocoon structure can explain the observed afterglow or a choked-jet cocoon (Lazzati et al. 2017b; Mooley et al. 2017).

The afterglow models presented here can be used with future EM jet-counterparts to GW detected NS mergers. For a Gaussian structured jet, the rising broad-band emission of the afterglow from $\sim$10 d depends on the inclination and the jet parameters, whereas for a cocoon model it should be fairly consistent for a wide range of observation angles. Failed GRB afterglows, or other jet structures could be revealed by further GW-EM detections.

ACKNOWLEDGEMENTS

The authors thank the anonymous referee, Iain A. Steele, Phil James, Dan Hoak, David Bersier, and Hendrik van Eerten for useful comments. This research was supported by Science Technology and Facilities Council grants. GPL was partially supported by International Astronomical Union and Royal Astronomical Society grants.

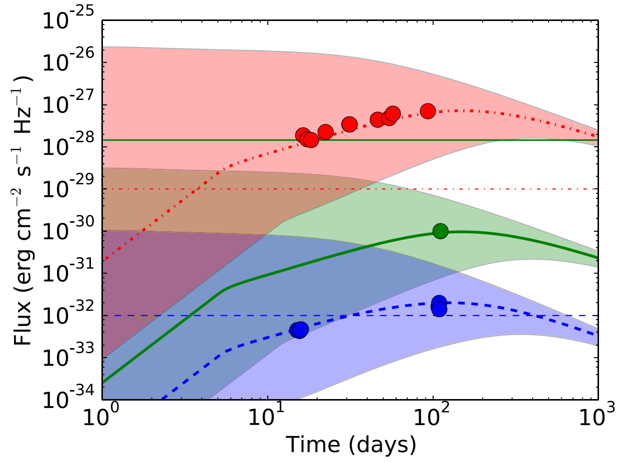

Figure 6. Afterglow from a modified Gaussian structured jet with parameters tuned to recreate the observed radio, optical, and X-ray observations if viewed at 20°. The afterglow range indicates the light curve for an inclination $10° \leq i \leq 26°$. X-ray at 1 keV is shown in blue, optical with green, and 3 GHz in red. Markers indicate observations from Hallinan et al. (2017), Haggard et al. (2017), Lyman et al. (2018), Margutti et al. (2017), Mooley et al. (2017), and Ruan et al. (2017); errorbars are typically smaller than the markers and not included.

REFERENCES

Abbott B. P. et al., 2016, Living Rev. Relativ., 19, 1
Abbott B. P. et al., 2017a, Phys. Rev. Lett., 119, 161101
Abbott B. P. et al., 2017b, ApJ, 848, L13
Abbott B. P. et al., 2017c, Nature, 551, 85
Arcavi I. et al., 2017, Nature, 551, 64
Barnes J., Kasen D., Wu M.-R., Martínez-Pinedo G., 2016, ApJ, 829, 110
Connaughton V. GBM-LIGO Group, et al., GBM-LIGO Group, 2017, GCN Circ., 21506
Corsi A., Halliana G., Mooley K., Frail D. A., Kasliwal M. M., Palliyaguru N. T., GROWTH, 2017, GCN Circ., 21815
Coulter D. A. et al., 2017, Science, 358, 1156
Covino S. et al., 2017, Nat. Astron., 1, 791
Cowperthwaite P. S. et al., 2017, ApJ, 848, L17
Daigne F., Mochkovitch R., 1998, MNRAS, 296, 275
Drout M. R. et al., 2017, Science, 358, 1570
Eichler D., Livio M., Piran T., Schramm D. N., 1989, Nature, 340, 126
Evans P. A. et al., 2017, Science, 358, 1565
Fong W., Berger E., Margutti R., Zauderer B. A., 2015, ApJ, 815, 102
Gall C., Hjorth J., Rosswog S., Tanvir N. R., Levan A. J., 2017, ApJ, 849, L19
Goldstein A. GBM-LIGO Group, et al., GBM-LIGO Group, 2017a, GCN Circ., 21528
Goldstein A. et al., 2017b, ApJ, 848, L14
Gottlieb O., Nakar E., Piran T., 2018, MNRAS, 473, 576
Haggard D., Nynka M., Ruan J. J., Kalogera V., Cenko S. B., Evans P., Kennea J. A., 2017, ApJ, 848, L25
Hallinan G. et al., 2017, Science, 658, 1579
Hascoët R., Beloborodov A. M., Daigne F., Mochkovitch R., 2014, ApJ, 782, 5
Hotokezaka K., Nissanke S., Hallinan G., Lazio T. J. W., Nakar E., Piran T., 2016, ApJ, 831, 190
Ioka K., Nakamura T., 2001, ApJ, 554, L163
Jin Z.-P. et al., 2017, ApJ, 857, 128

Kathirgamaraju A., Barniol Duran R., Giannios D., 2018, MNRAS, 473, L121
Kilpatrick C. D. et al., 2017, Science, 358, 1583
Kisaka S., Ioka K., Nakamura T., 2015, ApJ, 809, L8
Kisaka S., Ioka K., Kashiyama K., Nakamura T., 2017, preprint (arXiv:1711.00243)
Kluźniak W., Lee W. H., 1998, ApJ, 494, L53
Kobayashi S., 2000, ApJ, 545, 807
Kobayashi S., Sari R., 2000, ApJ, 542, 819
Kobayashi S., Sari R., 2001, ApJ, 551, 934
Kobayashi S., Piran T., Sari R., 1997, ApJ, 490, 92
Kobayashi S., Zhang B., Mészáros P., Burrows D., 2007, ApJ, 655, 391
Kopač D. et al., 2015, ApJ, 806, 179
Lamb G. P., Kobayashi S., 2016, ApJ, 829, 112
Lamb G. P, Kobayashi S., 2017, MNRAS, 472, 4953
Lazzati D., Deich A., Morsony B. J., Workman J. C., 2017a, MNRAS, 471, 1652
Lazzati D. et al., 2017b, preprint (arXiv:1712.03237)
Lyman J. D. et al., 2018, preprint (arXiv:1801.02669)
Mandel I., 2017, ApJ, 853, L12
Margutti R. et al., 2017, ApJ, 848, L20
Margutti R. et al., 2018, ApJ, 856, L18
Meng Y.-Z. et al., 2018, preprint (arXiv:1801.01410)
Meszaros P., Rees M. J., 1993, ApJ, 405, 278
Metzger B. D., Bauswein A., Goriely S., Kasen D., 2015, MNRAS, 446, 1115
Mooley K. P., Hallinan G., Corsi A., JAGWAR, GROWTH, 2017, GCN Circ., 21814
Mooley K. P. et al., 2017, Nature, 554, 207
Nakar E., Piran T., 2017, ApJ, 834, 28
Nicholl M. et al., 2017, ApJ, 848, L18
Paczynski B., 1990, ApJ, 363, 218
Pe'er A., Mészáros P., Rees M. J., 2006a, ApJ, 642, 995
Pe'er A., Mészáros P., Rees M. J., 2006b, ApJ, 652, 482
Perna R., Armitage P. J., Zhang B., 2006, ApJ, 636, L29
Phinney E. S., 1991, ApJ, 380, L17
Pian E. et al., 2017, Nature, 551, 67
Piron F., 2016, C. R. Phys., 17, 617
Planck Collaboration XIII, 2016, A&A, 594, A13
Riess A. G. et al., 2016, ApJ, 826, 56
Ruan J. J., Nynka M., Haggard D., Kalogera V., Evans P., 2017, ApJ, 853, L4,
Salafia O. S., Ghisellini G., Ghirlanda G., 2018, MNRAS, 474, L7
Sari R., Piran T., Narayan R., 1998, ApJ, 497, L17
Sari R., Piran T., Halpern J. P., 1999, ApJ, 519, L17
Savchenko V. INTEGRAL, et al., INTEGRAL, 2017a, GCN Circ., 21507
Savchenko V. et al., 2017b, ApJ, 848, L15
Shapiro S. L., 2017, Phys. Rev. D, 95, 101303
Shappee B. J. et al., 2017, Science, 358, 1574
Siellez K., Boer M., Gendre B., Regimbau T., 2016, preprint (arXiv:1606.03043)
Smartt S. J. et al., 2017, Nature, 551, 75
Tanaka M., 2016, Adv. Astron., 2016, 634197
Tanaka M., Hotokezaka K., Kyutoku K., Wanajo S., Kiuchi K., Sekiguchi Y., Shibata M., 2014, ApJ, 780, 31
Tanaka M. et al., 2017, PASJ, 69, 102
Tanvir N. R. et al., 2017, ApJ, 848, L27
Troja E. et al., 2017, Nature, 551, 71
Valenti S. et al., 2017, ApJ, 848, L24
Wollaeger R. T. et al., 2018, MNRAS, 000, 000
Xiao D., Liu L.-D., Dai Z.-G., Wu X.-F., 2017, ApJ, 850, L41
Yamazaki R., Ioka K., Nakamura T., 2002, ApJ, 571, L31
Yonetoku D., Murakami T., Tsutsui R., Nakamura T., Morihara Y., Takahasi K., 2010, PASJ, 62, 1495
Yu H.-F. et al., 2016, A&A, 588, A135
Zhang B., Kobayashi S., 2005, ApJ, 628, 315
Zhang B., Yan H., 2011, ApJ, 726, 90
Zhang F.-W., Shao L., Yan J.-Z., Wei D.-M., 2012, ApJ, 750, 88

This paper has been typeset from a TEX/LATEX file prepared by the author.